Chinese Chemical Letters 32 (2021) 2534–2538

Contents lists available at ScienceDirect

Chinese Chemical Letters

journal homepage: www.elsevier.com/locate/cclet

Communication

Facile defect engineering in $ZnIn_2S_4$ coupled with carbon dots for rapid diclofenac degradation

Dongxu Yang[a,b], Jialiang Liang[a,b], Liang Luo[a,b], Ruoyu Deng[a,b], Guo Li[a,b], Qiang He[a,b], Yi Chen[a,b,*]

[a] Key Laboratory of the Three Gorges Reservoir Region's Eco-Environment, Ministry of Education, Chongqing University, Chongqing 400045, China
[b] College of Environment and Ecology, Chongqing University, Chongqing 400045, China

ARTICLE INFO

Article history:
Received 31 August 2020
Received in revised form 2 December 2020
Accepted 26 December 2020
Available online 31 December 2020

Keywords:
Photocatalysis
Diclofenac degradation
Defect engineering
$ZnIn_2S_4$nanosheet
Carbon dots

ABSTRACT

Semiconductor-mediated photocatalysis is a promising photochemical process for harvesting inexhaustible solar energy to address the energy crisis and environmental issues. However, the low solar-light response and poor carrier migration are severe drawbacks that limit its practical application. Herein, we propose a convenient pathway for improving electron-hole separation and solar energy utilisation by engineering defective $ZnIn_2S_4$ with doping of carbon dots. The optimum $ZnIn_2S_4$/CD200 nanosheet exhibited 100% diclofenac (DCF) degradation within 12 min under visible-light. The estimated photocatalytic efficiency under natural sunlight was 98.2%. Scavenging experiments and electron spin resonance (ESR) analysis indicated that the superoxide radical ($O_2^{\bullet-}$), photoelectron (e^-), hole (h^+) and hydroxyl radical ($^{\bullet}OH$) were the predominant contributions in the $ZnIn_2S_4$/CD200/DCF/visible light system. Furthermore, $ZnIn_2S_4$/CD200 exhibited excellent reusability and stability after 4 times recycling. The photodegradation routes mainly involved hydroxylation, decarboxylation, C—N bond cleavage, dechlorination, ring closure, and ring-opening. The ecological risk assessment and total organic carbon (TOC) tests exhibited desirable toxicity reduction and mineralization results. These observations not only offer a facile strategy for the construction of defective $ZnIn_2S_4$, but also pioneer the direct utilisation of natural light for highly efficient environmental remediation.

In recent decades, pharmaceuticals, which have saved countless lives, have evolved into a new category of environmental pollutants [1]. Diclofenac (DCF) has been extensively employed for relieving pain, inflammation, and rheumatism and received consistent attention [2,3]. However, DCF enters various aqueous matrixes (such as surface water, groundwater, and even potable water) due to its recalcitrant chemical structure, and limited removal efficiency [4,5]. As a result, DCF poses a risk to human health and aquatic organisms, even at trace levels [6,7]. Therefore, it is vital that efficient and environmentally benign techniques for the practical remediation of resident DCF in wastewater.

Many strategies, including advanced oxidation processes [8], filtration [9], adsorption [10], plasma technique [11] and photocatalysis [12], have been developed for DCF removal. Among these excellent means, semiconductor-mediated photocatalysis has been developed as a promising chemical approach that converts solar energy into chemical energy to resolve the energy shortage and deteriorative environmental issues [13,14]. Nevertheless, the practical application of this process is hindered by its low photocatalytic activity due to the poor light-harvesting response and slow charge-hole migration [15]. Fortunately, the prosperity of two-dimensional materials offers new opportunities for the photocatalytic process. Recently, impressive two-dimensional g-C_3N_4/CQDs [3], $Cd_{0.9}Zn_{0.1}S/MoS_2$ [2], CQDs/BiOCOOH [4], Ag-BiOI-rGO [16], have received increasing attention for DCF degradation. However, the limited photodegradation efficiency could not meet practical requirements. The direct conversion of natural sunlight for efficiently degrading DCF has not yet been explored. Therefore, developing a highly efficient photocatalyst with facile preparation and rapid carrier migration that directly uses natural light should receive more attention.

As a ternary metal chalcogenide semiconductor, layered $ZnIn_2S_4$, which has a desirable bandgap and can adsorb visible light, has received ongoing attention [17,18]. However, narrow-

* Corresponding author at: Key Laboratory of the Three Gorges Reservoir Region's Eco-Environment, Ministry of Education, Chongqing University, Chongqing 400045, China.
E-mail address: chenyi8574@cqu.edu.cn (Y. Chen).

https://doi.org/10.1016/j.cclet.2020.12.049
1001-8417/

band-gap metal sulfide-photocatalysts are susceptible to photo-corrosion under solar light illumination, which is ubiquitous in most semiconductors [19]. Therefore, considerable effort has been devoted to suppressing the photo-induced instability of semiconductor materials. On one hand, defects engineering presents a promising platform for improving carrier separation and enhancing the performance of photocatalysis [20]. For example, the sulphur vacancy (*Vs*)-mediated defect behaviour in $ZnIn_2S_4$ can act as a trap for photo-generated electrons, which would accelerate the carrier transmission and improve H_2 production by 11 times [21]. Similar results were also reported by Du *et al.* [22], Li *et al.* [23] and He *et al.* [24]. It is thus reasonable to utilize $ZnIn_2S_4$ with defects as a photocatalyst matrix. At present, most studies employed the solvothermal route (temperature of approximately 180 °C for 12 or 24 h) to achieve $ZnIn_2S_4$ with defects [20–22]. However, information is scarce low-temperature (oil bath 80 °C) and rapid (2 h) defective $ZnIn_2S_4$ preparation. On the other hand, carbon dots (CD), which are *quasi*-spherical, zero-dimension nanoparticles (smaller than 10 nm), are a new generation of carbon nanomaterials for photocatalysis with unique physico-chemical and optical properties [25]. Additionally, CD exhibit prominent electron migration and reservoir behaviours. Consequently, CD can be embedded in semiconductors to enhance their photocatalytic efficiency and the utilisation of sunlight, such as TiO_2 [7], WO_3 [26], $ZnFe_2O_4$ [27], BiOCOOH [4], $BiPO_4$ [28], UiO-66 [29], Bi:TiO_2 [30] and $CuWO_4$/CdS [31]. However, few studies have been conducted on CD implanted with defective $ZnIn_2S_4$ and their application for highly-efficient DCF photo-degradation under visible light and natural sunlight.

In this study, we present a simple strategy for improving carrier migration and solar energy utilization by engineering $ZnIn_2S_4$ with defects and simultaneously incorporating CD. The composites exhibit excellent photocatalytic performance during the degradation of DCF under visible light and natural sunlight. This work aims to (1) develop a defective $ZnIn_2S_4$ composite *via* a facile method, (2) characterize and confirm the physicochemical and optical properties of photocatalysts, (3) explore the photo-degradation performance, mechanism, and (4) estimate the stability of the photocatalyst.

The profile and microstructure of the CD and $ZnIn_2S_4$/CD200 were determined by transmission electron microscopy (TEM). The high-resolution TEM (HRTEM) image of CD exhibits a quasi-spherical zero-dimensional nanostructure with an interplanar spacing of 0.219 nm (Fig. 1a and inset), which consistent with the (100) diffraction facets of graphite [25]. From the scanning electron microscopy (SEM) pattern in Fig. S1 (Supporting information), $ZnIn_2S_4$/CD200 exhibited a porous and complicated flake structure. Furthermore, Fig. 1b shows interconnected geometry with the nanosheet structure in the low-magnification TEM pattern, which agrees well with the SEM observations. The HRTEM images show the interplanar distance in the lattice fringes of the $ZnIn_2S_4$/CD200 (0.326 nm) and CD (0.219 nm), corresponding to the (102) facet of the $ZnIn_2S_4$/CD200 and (100) plane of CD (Fig. 1c) [32]. Clear atomic deficiencies are present on the $ZnIn_2S_4$/CD200, and the irregular lattice fringes in the yellow region and distortion in the blue range indicate that there are abundant defects in the $ZnIn_2S_4$/CD200 [33]. This result can be further verified by the electron spin resonance (ESR) analysis (Fig. 1d), demonstrating that the $ZnIn_2S_4$/CD200 contained more defects.

The phase and crystal structure of the parent $ZnIn_2S_4$ and its composites were confirmed by X-ray diffraction (XRD) (Fig. 2a). The pure $ZnIn_2S_4$ exhibited the characteristic bands of the hexagonal $ZnIn_2S_4$ phase at $2\theta = 21.2°$, 27.5°, 30.4°, 47.5°, 52.4° and 55.7°, which could be consistent with the crystal faces at (006), (102), (104), (110), (116) and (202), respectively [22,24]. There were no conspicuous changes in the diffraction peaks and intensities

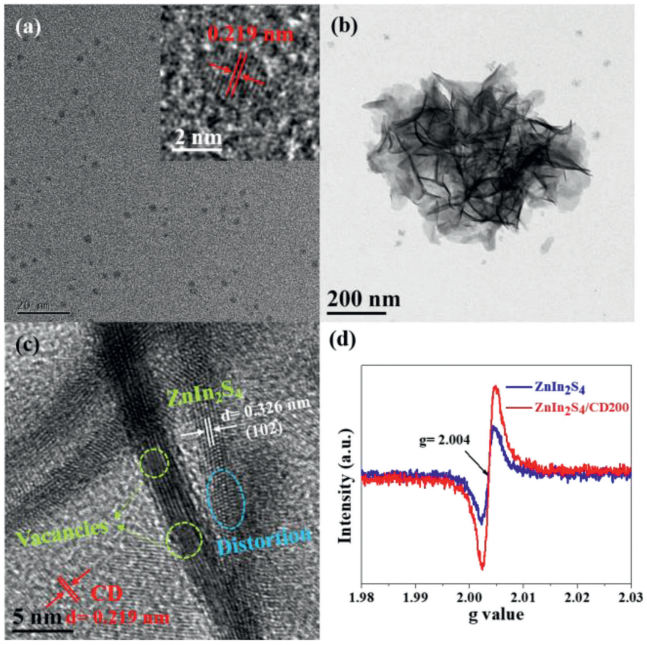

Fig. 1. TEM image of CD (a); TEM image (b), HRTEM image (c), and ESR spectra (d) of $ZnIn_2S_4$/CD200 nanosheet.

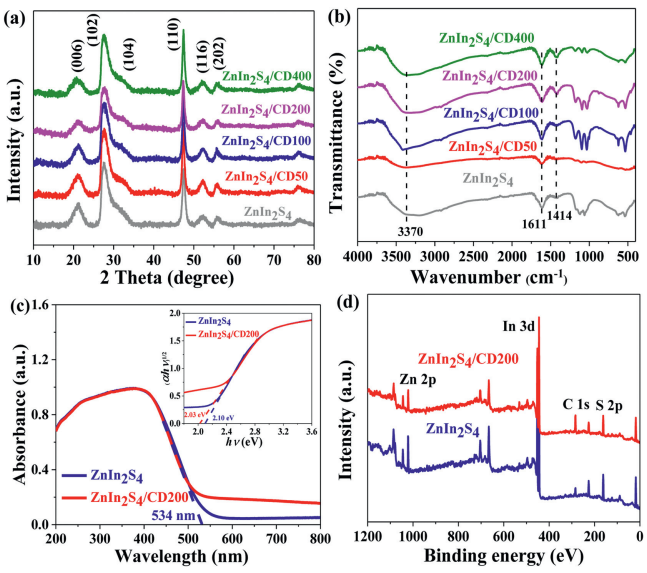

Fig. 2. XRD patterns (a), FT-IR spectra (b), DRS spectra (c) and XPS survey spectra of prepared samples (d).

after CD introduction, indicating the preservation of the pristine crystal structure and low CD concentration [28]. The FT-IR technique was employed to further validate the successful preparation of the catalysts. As shown in Fig. 2b, the parent $ZnIn_2S_4$ exhibited several adsorption bands at approximately 3370, 1611, and 1414 cm^{-1}, which could be associated with the hydroxyl units and absorbed water [20,34,35]. Additionally, the peaks at 1000–1250 cm^{-1} could be associated with the C—O bond in the residual solvent [36]. Similar profiles were also present in the serial $ZnIn_2S_4$/CD nanocomposites, demonstrating that the change in the chemical structure *via* CD doping was negligible [3,37]. The specific surface area of semiconductor catalysts plays an important role in their application as photocatalysis. Fig. S2 (Supporting information) and its inset present typical type-IV curves and the relevant

pore size distribution, respectively, and suggest the presence of a mesoporous framework. The parameters of the N_2 adsorption/desorption isotherms are listed in Table S1 (Supporting information). Defective $ZnIn_2S_4$ has a high specific surface area (106.18 m^2/g) and large pore volume (0.873 cm^3/g), surpassing those of most previously reported $ZnIn_2S_4$ catalysts [22,34]. The specific surface area of prepared material is not change much after CD loading, and they endow near degradation rates. Therefore, it can be predicted that the specific surface area is not the dominant factors influencing the photocatalytic performance that are controlled by doping and electron transfer [29,34]. The optical properties of the photocatalysts were recorded by UV–vis diffuse reflectance spectra (DRS). As shown in Fig. 2c, $ZnIn_2S_4$ and $ZnIn_2S_4$/CD200 exhibited similar absorption edges at approximately 534 nm, indicating that the photocatalysts can respond under visible-light. The absorption intensity of $ZnIn_2S_4$/CD200 was notably enhanced above 500 nm, suggesting the presence of the defect-state in the band structure [24]. The optical bandgaps can be determined *via* $(\alpha h\nu)^{1/2} = A(h\nu\text{-}E_g)$ equation [2].

According to the inset of Fig. 2c, the bandgaps of $ZnIn_2S_4$ and $ZnIn_2S_4$/CD200 are 2.10 and 2.03 eV, respectively. The Mott-Schottky (M-S) curve was used to confirm the type of photocatalyst. Fig. S3 (Supporting information) exhibits a positive slope for $ZnIn_2S_4$/CD200, which is consistent with n-type semiconductors [38,39]. The flat-band potential (E_f) of $ZnIn_2S_4$/CD200 is −0.93 eV *vs.* SCE, and reached −0.69 eV *vs.* normal hydrogen electrode (NHE). Therefore, the CB of $ZnIn_2S_4$/CD200 was −0.99 eV [38]. X-ray photoelectron spectroscopy (XPS) was employed to determine the elemental composition, chemical state, and presence of defects (Fig. 2). As shown in the XPS survey pattern (Fig. 2d), S, In, and Zn were present. The high-resolution S 2p spectra of $ZnIn_2S_4$ and $ZnIn_2S_4$/CD200 in Fig. S4a (Supporting information) exhibit two characteristic bands (S $2p_{1/2}$ and S $2p_{3/2}$) [24]. The negative shifts in the S $2p_{3/2}$ and S $2p_{1/2}$ peaks for $ZnIn_2S_4$/CD200 (161.49 and 162.69 eV) from those of $ZnIn_2S_4$ (161.59 and 162.85 eV) indicate the presence of defects [22]. Similarly, the Zn 2p binding energies and intensities for $ZnIn_2S_4$/CD200 (1044.44 eV, Zn $2p_{1/2}$ and 1021.38 eV, Zn $2p_{3/2}$) also exhibit similar contrasting reductive tendencies compared to those of $ZnIn_2S_4$ (1044.51 eV, Zn $2p_{1/2}$ and 1021.48 eV, Zn $2p_{3/2}$) [40]. However, there were no clear changes in the In 3d binding energy for $ZnIn_2S_4$ (452.29 eV, In $3d_{3/2}$ and 444.74 eV, In $3d_{5/2}$) when CD was present (452.28 eV, In $3d_{3/2}$ and 444.73 eV, In $3d_{5/2}$). These results indicated that the deficiency of S atoms resulted in reduced electron density at the nearby Zn atoms, rather than the nearby In atoms [21,24], indicating the occurrence of local electron transport. Further quantitative elemental analysis exhibited different atomic percentages (Table S2 in Supporting information). $ZnIn_2S_4$ exhibited sulfur-vacancy properties due to the Zn:In:S ratio of 1.02:2:3.42. Following the implantation of CD, the atomic ratio of Zn further declined, which could be due to the existence of Zn vacancies. This is consistent with the ESR results.

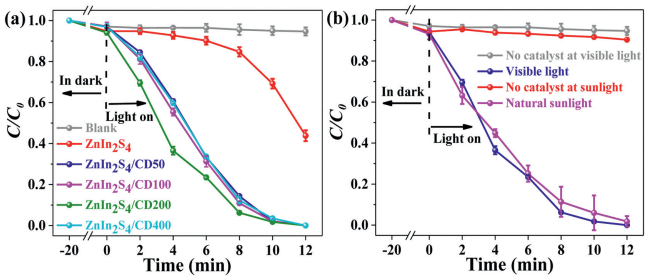

Fig. 3. Photocatalytic degradation of DCF under visible light on different photocatalysts (a). Photocatalytic activity of DCF under visible and natural light (b).

To estimate the photocatalytic activities of the materials, the photocatalytic DCF degradation process under visible light and natural sunlight were performed. Fig. 3a compares the DCF degradation achieved by the different photocatalysts. The absence of catalyst did not impact the DCF degradation under visible light. However, in the presence of parent $ZnIn_2S_4$ and its composites, the photocatalytic performance was greatly enhanced. In particular, $ZnIn_2S_4$/CD200 achieved optimal activity and fully removed the DCF within 12 min at a degradation rate of 0.455 min^{-1}, which is 15.7-fold that of $ZnIn_2S_4$ (Fig. S5 in Supporting information). Interestingly, the catalytic performance decreased after doping with a high amount of CD, indicating that the inner filter effect weakened the acquisition of photons by $ZnIn_2S_4$ [25,38]. Furthermore, we found that $ZnIn_2S_4$/CD200 can efficiently catalyse the degradation of DCF under natural sunlight (Fig. 3b). There was no significant change in the DCF degradation under natural sunlight when there was no catalyst. However, the photocatalytic efficiency was estimated to be 98.2% in the presence of $ZnIn_2S_4$/CD200. As stated above, we summarized DCF degradation performance of previous reports and the materials in the present study (Table S3 in Supporting information). The observations reveal that $ZnIn_2S_4$/CD200 is superior to that of the currently used photocatalysts.

Photo-electrochemical characterisation was employed to explore the enhanced DCF degradation performance of $ZnIn_2S_4$/CD200. The steady-state photoluminescence spectra (PL) in Fig. S6a (Supporting information) indicate evident PL quenching of $ZnIn_2S_4$/CD200 nanosheet, suggesting the suppressed recombination of electron-hole pair. The time-resolved photoluminescence (TRPL) spectra confirm the charge-carrier kinetics of $ZnIn_2S_4$ and $ZnIn_2S_4$/CD200 (Fig. S6b in Supporting information). $ZnIn_2S_4$/CD200 exhibited a shorter average lifetime (1.11 ns) than $ZnIn_2S_4$ (1.70 ns, Table S4 in Supporting information). The clear PL quenching and lifetime reduction reveal the efficient electron-hole migration behavior from $ZnIn_2S_4$ to CD in $ZnIn_2S_4$/CD200 nanosheet [41]. As shown in Fig. S6c (Supporting information), the EIS pattern displays a smaller semicircle for $ZnIn_2S_4$/CD200, suggesting lower charge migration resistance in this photocatalyst, which permits the slow recombination of photo-induced electron-hole pairs. Similarly, the enhanced carrier transfer dynamics of $ZnIn_2S_4$/CD200 were also proposed by the transient photocurrent

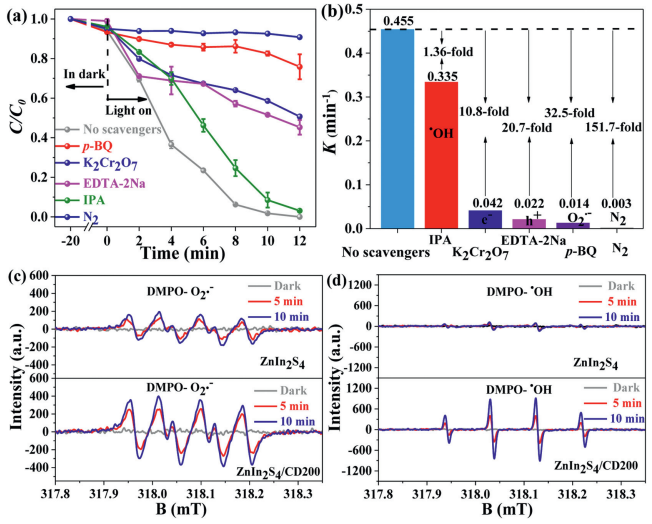

Fig. 4. Photocatalytic degradation of DCF with different scavengers (a), and corresponding rate constant (b), ESR spectra of DMPO-$O_2^{\bullet-}$ (c) and DMPO-$^{\bullet}OH$ (d) signals for $ZnIn_2S_4$ and $ZnIn_2S_4$/CD200.

measurements (Fig. S6d in Supporting information). These results indicate that the rich defects and CD implantation can significantly facilitate charge migration and the response to solar light.

To elucidate the contribution of reactive species, the trapping experiments were conducted (Fig. 4a). The photocatalytic efficiency of DCF decreased slightly when isopropyl alcohol (IPA) was introduced into the photo-reactor, and the degradation rate decreased from 0.455 to 0.335 min^{-1}. However, the participation of *p*-benzoquinone (*p*-BQ), potassium dichromate ($K_2Cr_2O_7$), and ethylenediaminetetraacetic acid disodium salt dihydrate (EDTA-2Na) greatly restrained the degradation rate of DCF under visible light. The rate constants are 32.5-fold, 10.8-fold, and 20.7-fold lower than those of the scavenger-free, respectively (Fig. 4b). The results suggest that $^{\bullet}OH$ plays a negligible role, e^- and h^+ play a secondary function, and $O_2^{\bullet-}$ is the predominant contributor to the photodegradation process [2]. DCF degradation process was not occurred in the oxygen-deficient environment, indicating that O_2 is indispensable for the degradation reaction. Moreover, the presence of $O_2^{\bullet-}$ and $^{\bullet}OH$ products on $ZnIn_2S_4$ and $ZnIn_2S_4$/CD200 was also directly confirmed by the ESR analysis. Figs. 4c and d presents the $O_2^{\bullet-}$ and $^{\bullet}OH$ generation signals by photocatalysts in the dark and under visible light (5 and 10 min). No clear $O_2^{\bullet-}$ (1:1:1:1) and $^{\bullet}OH$ (1:2:2:1) signal peaks were observed in the dark, while the signal intensities markedly enhanced under visible light as the illumination time increased. Additionally, the signal intensities of $O_2^{\bullet-}$ and $^{\bullet}OH$ of $ZnIn_2S_4$/CD200 are greater than those of $ZnIn_2S_4$. This indicates that $ZnIn_2S_4$ and $ZnIn_2S_4$/CD200 can generate $O_2^{\bullet-}$ and $^{\bullet}OH$, and $ZnIn_2S_4$/CD200 achieved higher electron-hole separation and utilisation of sunlight, corresponding to the photocatalysis results.

A schematic diagram of the proposed mechanism is shown in Fig. S7 (Supporting information). The $ZnIn_2S_4$/CD200 nanosheet can produce e^- and h^+ under visible-light. The photo-induced e^- on the CB of $ZnIn_2S_4$ can migrate to the CD due to the electronic storage characteristics of CD [27]. The energy band structure of $ZnIn_2S_4$/CD200 exhibited a more negative CB edge than the potential of $O_2/O_2^{\bullet-}$ (-0.33 eV *vs.* NHE). Therefore, the transferred e^- in the CD can cause O_2 to adsorb onto the surface of $ZnIn_2S_4$/CD200 to generate $O_2^{\bullet-}$ [42]. As shown in the ESR patterns, $^{\bullet}OH$ signal peaks were present, which was attributed to the multi-step transformation between e^- and O_2, rather than direct h^+ oxidation. This illustrated that $O_2^{\bullet-}$ was a rate-determining step under trapping experiment of $^{\bullet}OH$, thus leading to slight decrease of rate in IPA addition and obvious decline in *p*-BQ participation. According to the trapping test, h^+ and e^- also directly served as the contribution due to the formation of interstitial energy states, allowing more photogenerated e^-/h^+ to participate in the photocatalytic process. Moreover, the up-converted PL behaviour of CD resulted in stronger absorption of sunlight. Therefore, $ZnIn_2S_4$/CD200 achieved excellent DCF degradation under natural light. In summary, $O_2^{\bullet-}$, $^{\bullet}OH$, h^+, and e^- are synergistically responsible for the degradation of DCF.

To further explore the degradation mechanism, a series of DCF by-products and corresponding structures were recorded through LC–MS analysis (Table S5 in Supporting information). Based on these proposed intermediates, there were three possible degradation pathways of DCF by $ZnIn_2S_4$/CD200 under visible light, namely pathways A, B, and C (Fig. S8 in Supporting information). The *m/z* fragment of the intermediates increased in the first 6 min, then decreased as the irradiation time continued. This can be attributed to two reasons. The low-electron-density C-15 atoms in DCF could be preferentially attacked by nucleophilic $O_2^{\bullet-}$ to generate carbocation radicals, and further oxidized to produce **P1** (*m/z* 298) [4,7]. The C-4 atom in **P1** was then broken by $O_2^{\bullet-}$ to generate large-molecule **P2**. The small-molecule intermediate **P3** (*m/z* 181) was then generated by the cleavage of C—N bonds [2]. Pathway B involves the hydroxylation of DCF. The C-5 atom in DCF could form **P4** through hydroxylation due to its high-electron-density [43,44]. The structure of **P5** could be attributed to dihydroxylation, while **P6** was further hydroxylated with the loss of the chlorine atom [7,45]. The *m/z* 168 and 145 fragments are vital and agree well with the cleavage of the C—N bond through the attack of h^+ [2]. In pathway C, e^- can induce dechlorination and interact with $^{\bullet}OH$ to produce **P7** (*m/z* 241) [46], while $O_2^{\bullet-}$ could facilitate the oxidation of C-15 on **P7**, resulting in the formation of **P8** (*m/z* 211). Following decarboxylation and election reduction, **P9** (*m/z* 197) was detected [47]. These intermediates broke up into small-molecule by-products, and finally CO_2 and H_2O. The TOC analysis confirms the final fate of DCF in the $ZnIn_2S_4$/CD200 photocatalytic system. The TOC removal rate was calculated to be 48.62% within 12 min under visible-light illumination (Fig. S9a in Supporting information), indicating that the parent DCF and its related by-products can be decomposed by the reactive species and converted into CO_2 and H_2O.

Whether the intermediate of DCF degradation is environmentally friendly is related to human health. Therefore, the Toxicity Estimation Software Tool (T.E.S.T.) was used to determine the ecotoxicity risk of the photocatalytic products [3]. Fig. S9b (Supporting information) shows the effect of a lethal concentration of 50% (LC_{50}) in the fathead minnow (96 h) in the system with degradation intermediates. The LC_{50} value of the parent DCF is 0.43 mg/L. All degradation by-products exhibited a higher LC_{50} value (excluding **P4** and **P5**), indicating that the hydroxylation process has negative effects [48]. Among all intermediates, the larger-molecules intermediates resulted in a high degree of toxicity, while the small-molecule intermediates were less toxic, particularly **P10**, **P11**, **P12** and **P13**, as they were further oxidized and mineralized. Therefore, a high degree of oxidation and mineralization is vital to ensure safe water quality. Overall, the $ZnIn_2S_4$/CD200/visible light system could weaken the ecological toxicity of DCF to aquatic organisms.

Reusability and stability are important for assessing the performance of materials in a photocatalytic system. As shown in Fig. S9c (Supporting information), the degradation efficiency was 87% during the fourth recycle, suggesting a slight decrease in efficiency from the first experiment. The crystallinity of the fresh and reused $ZnIn_2S_4$/CD200 was compared using their XRD patterns (Fig. S9d in Supporting information). No clear phase changes can be observed, and these observations confirm the excellent regeneration and stability of $ZnIn_2S_4$/CD200.

In summary, we successfully synthesised defective $ZnIn_2S_4$/CD200 nanosheets *via* a facile method. The development of defects and implantation of CD can introduce interstitial states to extend the carriers' recombination pathways and provide a charge-transfer channel to migrate e^- from $ZnIn_2S_4$ to CD. More photoinduced e^- and h^+ can participate in the photocatalytic system, thereby achieving a 100% removal percentage and rate constant of 0.455 min^{-1} for DCF degradation. The photocatalytic efficiency was estimated to be 98.2% under natural sunlight. $O_2^{\bullet-}$, e^-, h^+ and $^{\bullet}OH$ play key roles in DCF degradation. Hydroxylation, decarboxylation, C—N bond cleavage, dechlorination, ring closure, and ring-opening are the main DCF photodegradation pathways. The ecological risk assessment shows that $ZnIn_2S_4$/CD200/visible light system could weaken the ecological toxicity of DCF to aquatic organisms. These findings indicate that the engineering of defects and incorporation of carbon dots can accelerate electron migration and direct use of natural-sunlight for environmental remediation and other applications.

Declaration of competing interest

The authors report no declarations of interest.

Acknowledgments

This work was funded by the Venture & Innovation Support Program for Chongqing Overseas Returnees (No. cx2019034) and National Major Project of Pollution Control and Treatment Science and Technology (No. 2017ZX07401003-4). We would also like to thank the Analytical and Testing Center of Chongqing University for conducting the various characterization.

Appendix A. Supplementary data

Supplementary material related to this article can be found, in the online version, at doi:https://doi.org/10.1016/j.cclet.2020.12.049.

References

[1] M. Patel, R. Kumar, K. Kishor, et al., Chem. Rev. 119 (2019) 3510–3673.
[2] M. Cai, R. Li, Z. Xie, et al., Appl. Catal. B 259 (2019) 118033.
[3] W. Liu, Y. Li, F. Liu, et al., Water Res. 151 (2019) 8–19.
[4] P. Chen, Q. Zhang, Y. Su, et al., Chem. Eng. J. 332 (2018) 737–748.
[5] M.O. Barbosa, N.F. Moreira, A.R. Ribeiro, M.F. Pereira, A.M. Silva, Water Res. 94 (2016) 257–279.
[6] Z. Hu, X. Cai, Z. Wang, et al., J. Hazard. Mater. 380 (2019) 120812.
[7] F. Wang, Y. Wu, Y. Wang, et al., Chem. Eng. J. 356 (2019) 857–868.
[8] Y. Su, D. Jassby, S. Song, et al., Environ. Sci. Technol. 52 (2018) 6466–6475.
[9] H. Kohay, A. Izbitski, Y.G. Mishael, Environ. Sci. Technol. 49 (2015) 9280–9288.
[10] B.N. Bhadra, I. Ahmed, S. Kim, S.H. Jhung, Chem. Eng. J. 314 (2017) 50–58.
[11] R. Deng, Q. He, D. Yang, et al., Chem. Eng. J. 406 (2021) 126884.
[12] Y. Cui, Q. Ma, X. Deng, et al., Appl. Catal. B 206 (2017) 136–145.
[13] B. Dong, T. Liu, C. Li, F. Zhang, Chin. Chem. Lett. 29 (2018) 671–680.
[14] B. Li, L. Nengzi, R. Guo, et al., Chin. Chem. Lett. 31 (2020) 2705–2711.
[15] P. Wang, Y. Mao, L. Li, et al., Angew. Chem. Int. Ed. 131 (2019) 11451–11456.
[16] W. Li, R. Yu, M. Li, et al., Chemosphere 218 (2019) 966–973.
[17] Y. Pan, X. Yuan, L. Jiang, et al., Chem. Eng. J. 354 (2018) 407–431.
[18] H. Yang, R. Cao, P. Sun, et al., Appl. Catal. B 256 (2019) 117862.
[19] B. Weng, M.Y. Qi, C. Han, Z.R. Tang, Y.J. Xu, ACS Catal. 9 (2019) 4642–4687.
[20] X. Jiao, Z. Chen, X. Li, et al., J. Am. Chem. Soc. 139 (2017) 7586–7594.
[21] S. Zhang, X. Liu, C. Liu, et al., ACS Nano 12 (2017) 751–758.
[22] C. Du, Q. Zhang, Z. Lin, et al., Appl. Catal. B 248 (2019) 193–201.
[23] Z. Li, J. Hou, B. Zhang, et al., Nano Energy 59 (2019) 537–544.
[24] Y. He, H. Rao, K. Song, et al., Adv. Funct. Mater. 29 (2019) 1905153.
[25] F. Wang, P. Chen, Y. Feng, et al., Appl. Catal. B 207 (2017) 103–113.
[26] J. Zhang, J. Liu, X. Wang, et al., Appl. Catal. B 259 (2019) 118063.
[27] Y. Huang, Y. Liang, Y. Rao, et al., Environ. Sci.Technol. 51 (2017) 2924–2933.
[28] Q. Zhang, P. Chen, M. Zhuo, et al., Appl. Catal. B 221 (2018) 129–139.
[29] X. Peng, L. Ye, Y. Ding, et al., Appl. Catal. B 260 (2020) 118152.
[30] J. Li, C. Zhong, J. Huang, et al., J. Colloid Interf. Sci. 553 (2019) 758–767.
[31] Y. Chen, J. Li, P. Liao, et al., Chin. Chem. Lett. 31 (2020) 1516–1519.
[32] G. Yang, D. Chen, H. Ding, et al., Appl. Catal. B 219 (2017) 611–618.
[33] W. Yang, L. Zhang, J. Xie, et al., Angew. Chem. Int. Ed. 55 (2016) 6716–6720.
[34] Q. Zhu, Y. Sun, S. Xu, et al., J. Hazard. Mater. 382 (2020) 121098.
[35] D. Yang, J. Li, L. Luo, et al., Chem. Eng. J. 387 (2020) 124103.
[36] B. Gao, L. Liu, J. Liu, F. Yang, Appl. Catal. B 129 (2013) 89–97.
[37] F. Wang, Y. Wang, Y. Feng, et al., Appl. Catal. B 221 (2018) 510–520.
[38] Z. Xie, Y. Feng, F. Wang, et al., Appl. Catal. B 229 (2018) 96–104.
[39] C. Chang, H. Yang, W. Mu, et al., Appl. Catal. B 254 (2019) 647–658.
[40] S. He, C. Yan, X. Chen, et al., Appl. Catal. B 276 (2020) 119138.
[41] M. Yang, Y. Xu, W. Lu, et al., Nat. Commun. 8 (2017) 14224.
[42] P. Chen, F. Wang, Z. Chen, et al., Appl. Catal. B 204 (2017) 250–259.
[43] C. Yi, Q. Liao, W. Deng, et al., Sci. Total Environ. 684 (2019) 527–536.
[44] H. Yu, E. Nie, J. Xu, et al., Water Res. 47 (2013) 1909–1918.
[45] S. Salaeh, D. Juretic Perisic, M. Biosic, et al., Chem. Eng. J. 304 (2016) 289–302.
[46] C. Martínez, M. Canle L, M.I. Fernández, J.A. Santaballa, J. Faria, Appl. Catal. B 107 (2011) 110–118.
[47] S. Li, Z. Wang, X. Zhang, et al., Chem. Eng. J. 378 (2019) 122169.
[48] Z. Cai, X. Hao, X. Sun, et al., Water Res. 162 (2019) 369–382.